Biophysical Journal
Article

Biophysical Society

Retinal Configuration of *p*pR Intermediates Revealed by Photoirradiation Solid-State NMR and DFT

Yoshiteru Makino,[1] Izuru Kawamura,[1,*] Takashi Okitsu,[2] Akimori Wada,[2] Naoki Kamo,[3] Yuki Sudo,[4] Kazuyoshi Ueda,[1,*] and Akira Naito[1,*]

[1]Graduate School of Engineering, Yokohama National University, Hodogaya-ku, Yokohama, Japan; [2]Laboratory of Organic Chemistry for Life Science, Kobe Pharmaceutical University, Higashinada-ku, Kobe, Japan; [3]Faculty of Advanced Life Science, Hokkaido University, Kita-ku, Sapporo, Japan; and [4]Graduate School of Medicine, Dentistry and Pharmaceutical Sciences, Okayama University, Okayama, Japan

ABSTRACT *Pharanois* phoborhodopsin (*p*pR) from *Natronomonas pharaonis* is a transmembrane photoreceptor protein involved in negative phototaxis. Structural changes in *p*pR triggered by photoisomerization of the retinal chromophore are transmitted to its cognate transducer protein (*p*HtrII) through a cyclic photoreaction pathway involving several photointermediates. This pathway is called the photocycle. It is important to understand the detailed configurational changes of retinal during the photocycle. We previously observed one of the photointermediates (M-intermediates) by in situ photoirradiation solid-state NMR experiments. In this study, we further observed the ^{13}C cross-polarization magic-angle-spinning NMR signals of late photointermediates such as O- and N′-intermediates by illumination with green light (520 nm). Under blue-light (365 nm) irradiation of the M-intermediates, ^{13}C cross-polarization magic-angle-spinning NMR signals of 14- and 20-^{13}C-labeled retinal in the O-intermediate appeared at 115.4 and 16.4 ppm and were assigned to the 13-*trans*, 15-*syn* configuration. The signals caused by the N′-intermediate appeared at 115.4 and 23.9 ppm and were assigned to the 13-*cis* configuration, and they were in an equilibrium state with the O-intermediate during thermal decay of the M-intermediates at −60°C. Thus, photoirradiation NMR studies revealed the photoreaction pathways from the M- to O-intermediates and the equilibrium state between the N′- and O-intermediate. Further, we evaluated the detailed retinal configurations in the O- and N′-intermediates by performing a density functional theory chemical shift calculation. The results showed that the N′-intermediate has a 63° twisted retinal state due to the 13-*cis* configuration. The retinal configurations of the O- and N′-intermediates were determined to be 13-*trans*, 15-*syn*, and 13-*cis*, respectively, based on the chemical shift values of [20-^{13}C] and [14-^{13}C] retinal obtained by photoirradiation solid-state NMR and density functional theory calculation.

INTRODUCTION

Pharaonis phoborhodopsin (*p*pR), also called sensory rhodopsin II (SRII), is a membrane protein isolated from the halophilic and alkaliphilic archaeal *Natronomonas pharaonis* that consists of seven-transmembrane α-helices with a vitamin-A aldehyde retinal as a chromophore (1). All-*trans* retinal is predominantly incorporated into the apoprotein of *p*pR. *p*pR functions as a photoreceptor protein by forming a 2:2 complex with the cognate two-helix transducer protein *p*HtrII to transmit the photosignal into the cytoplasm (2–5). The *p*pR/*p*HtrII complex is involved in negative phototaxis through a cyclic photoreaction pathway called the photocycle. In the initial state, *p*pR has an absorbance maximum at 498 nm in the ground (G) state under dark conditions. Light absorption transforms *p*pR from the ground state (ppR$_G$) to a K (540 nm)-intermediate with an absorbance maximum of 540 nm. This transformation is initiated by *trans*/*cis* photoisomerization of the retinal. The photocycle is followed by several intermediates, such as L (498 nm), M (390 nm), and O (560 nm), undergoing thermal relaxation processes. Finally, the O-intermediate thermally returns to the ppR$_G$ state (6).

The K-intermediate has a half-life of ∼1 μs, and its retinal is in the 13-*cis*, 15-anti configuration. Transformation of the K-intermediate provides the L-intermediate, which has a half-life of ∼30 μs and a 13-*cis*, 15-anti retinal configuration. Subsequently, a proton is removed from the Schiff base (SB) of the L-intermediate, resulting in transformation to the M-intermediate, which has a long half-life of ∼1.7 s.

Submitted March 6, 2018, and accepted for publication May 16, 2018.

*Correspondence: izuruk@ynu.ac.jp or ueda-kazuyoshi-cz@ynu.ac.jp or naito@ynu.ac.jp

Editor: Timothy Cross.

https://doi.org/10.1016/j.bpj.2018.05.030

The M-intermediate has a 13-*cis*, 15-anti retinal configuration with a deprotonated SB. Upon reprotonation, the M-intermediate transforms into the O-intermediate with a protonated SB, which has a half-life of ~770 ms and a 13-*trans*, 13-*syn* retinal configuration (4–7). The M- and O-intermediates have long half-lives as compared with the K- and L-intermediates, and thus they are known as late-active intermediates.

Important signal transduction processes such as changes in protein structure are induced at the late step in the photocycle. These changes likely include the formation of two specific hydrogen bonds, one between Tyr199$^{p\text{pR}}$ and Asn74$^{p\text{HtrII}}$ and one between Thr189$^{p\text{pR}}$ and Glu43$^{p\text{HtrII}}$/Ser62$^{p\text{HtrII}}$, as observed in the crystal structure of the *p*pR/*p*HtrII complex in the dark state (8) and K and M states (9,10). Thr204 is another important residue in *p*pR and plays a role in color tuning and in the photocycle kinetics of *p*pR (11). Further observations have shown that Thr204 is indispensable for the negative phototaxis function of the complex (12). There is steric hindrance in the K-intermediate between the C_{14}-H of retinal and Thr204 (13). At the same time, a specific hydrogen bond alteration occurs between Thr204 and Tyr174 in a *p*HtrII-dependent manner (12). Helix movement in *p*pR and outward tilting of helix F during the photocycle have been suggested by various groups (14–16) and are believed to be essential steps for the activation of *p*HtrII. However, no helix tilting was observed in the crystal structure of the M-intermediate of the *p*pR/*p*HtrII complex (9). After tilting of the F-helix in *p*pR, TM2 in *p*HtrII rotates, transferring the signal to the phosphorylation cascade to initiate rotation of the bacterial flagellar motor, resulting in negative phototaxis.

The photocycle as described above depends on the photoisomerization of retinal. The retinal chromophore in *p*pR forms a covalent bond with a perfectly conserved Lys residue (Lys205) bonded to an SB. Animal rhodopsin (type II rhodopsin) photobleaches, whereas microbial rhodopsin (type I rhodopsin) retains the retinal through the photocycle. Therefore, continuous irradiation of *p*pR with green light results in repeated photocycles without photobleaching, and the photointermediates can be trapped in a stationary state using type I rhodopsins such as *p*pR (1,5,17).

Photoirradiation solid-state NMR spectroscopy has been used to reveal the photoactivated intermediates of retinal membrane proteins. For example, photoactivated intermediates have been characterized by ^{13}C NMR studies of [^{13}C] retinal and ^{15}N NMR studies of [ζ-^{15}N]Lys of bacteriorhodopsin (bR) (18–21). The light-adapted state and the M- and N-intermediates of bR have been investigated using photoirradiation solid-state NMR spectroscopy (19,20). The early M-intermediate, M_0, and late M-intermediate, M_n, in the bR photocycle have been characterized by in situ photoirradiation solid-state NMR spectrometry (22–24). The combination of NMR spectroscopy with a dynamic nuclear polarization method revealed the heterogeneity of dark-adapted bR and distortion in the K-intermediate, and four discrete L-intermediates were detected (25,26). In addition to bR, the photoactive site of channelrhodopsin-2 was revealed (27). Thus, we have developed an in situ photoirradiation solid-state NMR apparatus that allows irradiation of the sample with extremely high efficiency and enables observation of the photointermediates and photoreaction processes of photoreceptor membrane proteins (28–35).

We previously trapped several photointermediates in the photostationary state using in situ photoirradiation solid-state NMR and observed the M-intermediates of *p*pR under green-light irradiation (29). Continuous irradiation of *p*pR with green light (520 nm) resulted in the accumulation of late-active intermediates such as multiple M-intermediates (M1, M2, and M3) because of their long lifetimes as compared with the early photointermediates such as the K- and L-intermediates. Generally, the half-lives of the late intermediates of sensory-type rhodopsin are much longer than that of ion-pump-type rhodopsins such as bR (5). It is reasonable that the longer half-life time of the photointermediates in sensory rhodopsins are accompanied by dynamic conformational changes to allow signal transmission to the transducer protein and signal amplification during the photocycle, whereas the fast photocycle is advantageous for transporting ions during the photocycle of ion-pump-type rhodopsins.

In this study, we focus on observing the late photointermediates after the M- intermediates by performing in situ photoirradiation solid-state NMR measurements using two light-emitting diode (LED) light sources, one each at 520 nm (green light) and 365 nm (blue light). We previously showed that the ^{13}C NMR signal from [20-^{13}C] retinal responds sensitively to changes in the 13C=14C configuration in retinal. Similarly, the ^{13}C NMR signal from [14-^{13}C] retinal should be sensitive to changes in the 15C=Nζ configuration in retinal. Here, we specifically detected the ^{13}C NMR signal from [14, 20-^{13}C]-labeled retinal in *p*pR. Based on the chemical shift values for [20-^{13}C] and [14-^{13}C] retinal in the late-active intermediates and the results of density functional theory (DFT) calculations, we discuss the detailed configurations of these intermediates.

MATERIALS AND METHODS

Sample preparation

[14, 20-^{13}C]-labeled retinal-*p*pR with a His-tag (6×His) at the C-terminal was overexpressed in *Escherichia coli* BL21(DE3) strain (Nippon Genetics, Toyama, Japan) in lysogeny broth medium by induction with 1 mM isopropyl-1-thio-β-D-galactoside (FUJIFILM Wako Pure Chemical Corporation, Tokyo, Japan) and 10 μM [14, 20- ^{13}C]-labeled all-*trans* retinal (synthesized by T.O. and A.W.). Protein expression was performed at 25°C for 15 hr. To purify the sample, the cells were lysed by ultrasonication, then the proteins were solubilized using n-dodecyl-β-D-maltoside (DDM) (Dojindo Laboratories, Kumamoto, Japan) and purified with Ni-NTA column (QIAGEN, Hilden, Germany) as previously described (29,36,37). *p*HtrII

(1–159) was also prepared by the same method as described previously (29). After purification, *p*pR was mixed with *p*HtrII at a 1:1 molar ratio by electrophoresis and by monitoring ultraviolet (UV)-visible absorption and thermal stability (38) of the *p*pR/*p*HtrII complex. The complex was reconstituted into membrane using DDM micelles incorporating a lipid film of L-α-egg-phosphatidylcholine (egg-PC) (Avanti Polar Lipids, Alabaster, AL) (*p*pR:egg-PC molar ratio of 1:30), then DDM was removed by using Bio-Beads (Bio-RAD, Hercules, CA). The reconstituted samples were suspended in 5 mM HEPES (Dojindo Laboratories), 10 mM NaCl buffer solution (pH 7) to provide *p*pR and *p*pR/*p*HtrII complex embedded in egg-PC lipid bilayers.

Solid-state NMR experiments

The fully hydrated sample was concentrated by centrifugation so that the molar ratio of water:lipid:protein reached 8350:30:1 with a hydrated ratio of 300%. Consequently, 66 mg of hydrated sample with 9 mg of protein was packed into a 5.0-mm-outer-diameter zirconia pencil-type rotor with a tightly sealed glass cap (JEOL Ltd., Akishima, Japan). Solid-state NMR experiments were performed on a CMX-400 Infinity (Chemagnetics, Fort Collins, CO) solid-state NMR spectrometer equipped with an in situ photoirradiation NMR system using resonance frequencies of 400 and 100 MHz for ^{1}H and ^{13}C nuclei, respectively. ^{13}C cross-polarization magic-angle-spinning (CP-MAS) experiments (39) were performed using the following conditions: ^{13}C 90° pulse of 5.4 μs, ^{1}H decoupling amplitude of 50 kHz, temperatures of −40 and −60°C, and a MAS frequency of 4.0 kHz. Two-pulse phase modulation proton high-power decoupling (40) was employed during each acquisition. Typically, 40,000 transients were accumulated for ∼44 hr to obtain each 1D CP-MAS NMR spectrum. ^{13}C chemical shifts were referenced to the carbonyl resonance of glycine powder at 176.03 ppm (tetramethylsilane (TMS) at 0.0 ppm).

In situ photoirradiation solid-state NMR measurements

In situ continuous photoirradiation was carried out using an optical fiber passed from outside the magnet through a tightly sealed glass cap made from a glass rod glued to a zirconia rotor (29,30,33). The glass rod was grained so as to provide illumination perpendicular to the rotor wall. The fluid membrane proteins were attached to the side wall of the rotor as a thin film and then light was directed perpendicular to the rotor wall from inside the spinner. If the irradiation is not perpendicular to the rotor wall, the light is completely reflected off the surface of the film sample and does not penetrate into the sample. The use of a CMX-400 Infinity NMR spectrometer (Chemagnetics) equipped with this photoirradiation system allowed us to efficiently irradiate samples in the rotor with green (520 nm) and blue (365 nm) LED light sources.

Stationary trapping of photointermediates using in situ photoirradiation solid-state NMR

In situ photoirradiation is particularly useful for studying the photocycle of several retinal binding membrane proteins. The half-life of the M-intermediate in *p*pR is ∼1.7 s, which is much longer than that of the other intermediates, as shown in Fig. 1 *A*. Thus, continuous irradiation of a sample with green light (520 nm) (*Green*) traps the M-intermediates in a stationary fashion as schematically shown in Fig. 1 *Bb*, making it possible to detect relatively short-lived intermediates in the stationary state when their half-life differs from those of other intermediates. After the green light is turned off (*Dark2*), the M-intermediates relax to the G state (Fig. 1 *Bc*). A difference spectrum between Green and Dark1 that is observed in the dark condition (Fig. 1 *Ba*) (*Green* − *Dark1*; Fig. 1 *Bd*) indicates the photoreaction pathway from Dark1 to Green and shows that the G state is transformed to the M-intermediate. Namely, a negative peak shows the reactant, and the positive peak shows the product. Similarly, the thermal relaxation process from Green to Dark2 is shown in the difference spectrum subtracting Green from Dark2 (*Dark2* − *Green*; Fig. 1 *Be*), which indicates that the M-intermediate is transformed to the G state.

The trapping efficiency can be increased by decreasing the temperature, because the photoreaction is a thermal process except for the photoillumination process (G → K), and therefore lowering the temperature extends the half-life of the M-intermediates. The M-intermediates can be eliminated by illuminating with 365 nm LED light, because the M-intermediates have a maximal absorbance frequency of 390 nm, which is different from the absorbance frequencies of the other intermediates. The M-intermediates can therefore be selectively eliminated by directly irradiating with 365 nm blue light, allowing detection of the activation of consecutive photoreaction processes such as the double-photon process by illuminating with multiple wavelengths. It is thus possible to select a particular intermediate by adjusting either temperature or wavelength.

Computing method to evaluate the ^{13}C chemical shift values of retinal

^{13}C chemical shifts of backbone Cα, C=O, and sidechain Cβ signals are significantly displaced for a variety of amino acid residues in polypeptides and proteins depending on their local conformation such as α-helix, β-sheet, or random coil (41). ^{13}C chemical shifts of [20-^{13}C] retinal are correlated with 13-*cis*/*trans* of 13C=14C configuration, and those of [14-^{13}C] retinal are correlated with 15-*syn*/anti of 15C=Nζ configuration, as experimentally obtained from various retinal proteins and summarized in Table S1. Here, we calculate the ^{13}C chemical shift values of retinal carbons to elucidate the relation between the ^{13}C chemical shift values and retinal configuration.

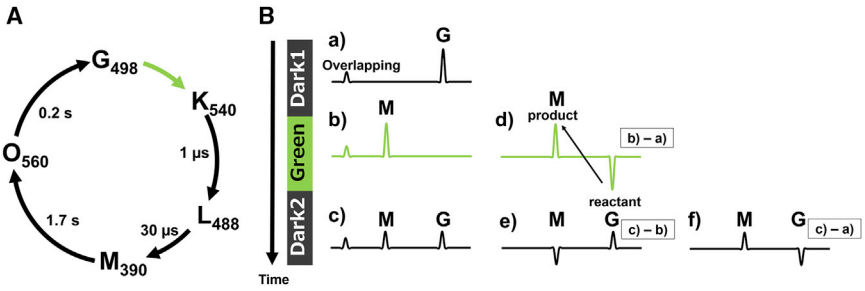

FIGURE 1 (*A*) Typical photocycle of the *p*pR/*p*HtrII complex. The M- and O-intermediates have much longer half-lives than the K- and L-intermediates. (*B*) The schematic experimental protocol and analysis strategy are shown. First, in situ photoirradiation solid-state NMR spectrum of the G state was observed in the dark state (*Dark1*) (*Ba*), then the spectrum of the M-intermediate under illumination with green light (*Green*) (*Bb*), and finally in the second dark state (*Dark2*) (*Bc*), in which the M-intermediate decreases and the G state increases. We analyzed the photoreaction pathway and eliminated overlapping signals by obtaining the difference spectra. The difference spectra shown are: (*Bd*) = (*Bb*) − (*Ba*), showing that the G state is transformed to the M-intermediate; (*Be*) = (*Bc*) − (*Bb*), showing that the M-intermediate is transformed to the G state; (*Bf*) = (*Bc*) − (*Ba*), showing that the G state is transformed to the M-intermediate. A negative peak in a difference spectrum indicates the reactant, and a positive peak indicates a product. To see this figure in color, go online.

The ^{13}C chemical shift calculations were performed using the gauge-independent atomic orbital method (42–46) in the Gaussian09 (47) program with the B3LYP/6-311+g** theory/basis set combination. The calculated chemical shifts were converted to ppm relative to TMS. A schematic structure of retinal, used in the chemical shift calculation, is shown in Fig. 2. Retinal binds to the protein through the side chain of Lys 205, as shown in Fig. 2. The SB was considered to be protonated in the calculation. The initial structure of the retinal was in the all-*trans* configuration of the crystal structure (Protein Data Bank (PDB): 1JGJ) (48), which corresponds to the G-state configuration. We investigated the configurations of the O- and N′-intermediates by evaluating the dependence of the ^{13}C NMR chemical shift on the configuration of retinal according to the rotation of the dihedral angles of 12C-13C=14C-15C, 14C-15C=Nζ-Cε, and 15C=Nζ-Cε-Cδ, abbreviated Φ, Ψ, and X, respectively (Fig. 2). The geometries of the heavy atoms of retinal were fixed in each dihedral angle, and only the hydrogen atoms were optimized with the same theory/basis-set conditions before calculation of the chemical shift values. The basis-set dependence of the calculation of chemical shift was examined for the G state of retinal using several basis sets. The results are shown in Table S2. It shows that the calculated values are almost the same as those in these large basis sets. In this work, the largest basis set of 6–311 + G** in the table was used in all the calculation.

RESULTS AND DISCUSSION

Photoreaction pathways under green-light irradiation of the *p*pR/*p*HtrII complex

In situ photoirradiation solid-state ^{13}C CP-MAS measurements were performed on the [20-^{13}C]-labeled retinal-*p*pR/*p*HtrII complex at −40°C. We obtained the photoreaction pathways under illumination with green light by first observing the ^{13}C CP-MAS NMR spectrum of the *p*pR/*p*HtrII complex in the dark condition (*Dark1*) at −40°C (Fig. 3 *Aa*; Fig. S1 *Aa* for *full spectrum*) and then the ^{13}C CP-MAS spectrum under illumination with 520 nm green light (Fig. 3 *Ab*; Fig. S1 *Ab* for *full spectrum*) to observe the intermediates in stationary state.

The [20-^{13}C] retinal signals shown in Fig. 3 *Aa* and *b* heavily overlapped with the lipid signals. The difference spectrum (*Green* − *Dark1*) was therefore obtained as shown in Fig. 3 *Ad* and Fig. S1 *Ad* for full spectrum to analyze the photoreaction pathways induced by photoirradiation. The difference spectrum between the light and dark states indicated that the negative peaks correspond to the reactant state and the positive peaks correspond to the product state. Thus,

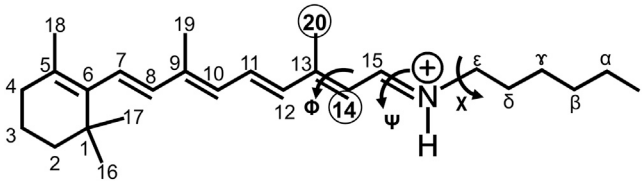

FIGURE 2 Schematic structure of retinal covalently bonded through an SB. The letters α, β, γ, δ, and ε are the positions of the carbons of Lys205 in *p*pR. The circled numbers are the positions of carbons observed by ^{13}C CP-MAS solid-state NMR. The dihedral angles Φ, Ψ, and X are defined as 12C-13C=14C-15C, 14C-15C=Nζ-Cε, and 15C=Nζ-Cε-Cδ, respectively.

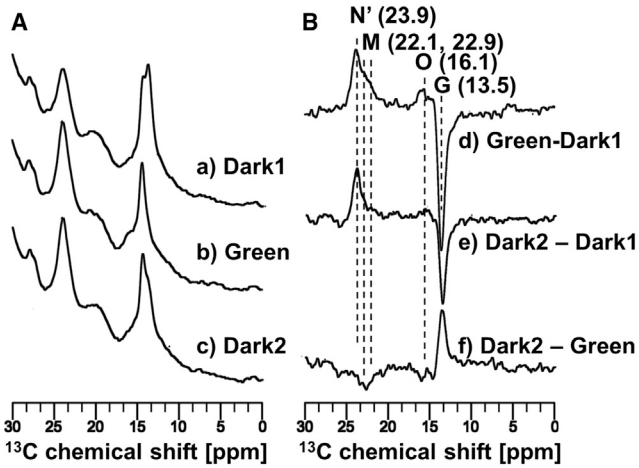

FIGURE 3 (*A*) ^{13}C CP-MAS NMR spectra of the [20-^{13}C] retinal–*p*pR/*p*HtrII complex at −40°C using a 4 kHz MAS frequency, (*a*) acquired under initial dark conditions (*Dark1*), (*b*) acquired under irradiation with green light (520 nm) (*Green*), and (*c*) obtained one day after turning off irradiation (*Dark2*). (*B*) The difference spectra obtained by (*d*) Green − Dark1 (process from *Dark1* to *Green*), (*e*) Dark2 − Dark1 (process from *Dark1* to *Dark2*), and (*f*) Dark2 − Green (process from *Green* to *Dark2*) are shown.

the ^{13}C CP-MAS NMR signal of the G state at 13.5 ppm decreased, and those of the M-intermediates at 22.1 and 22.9 ppm (M1 and M2), the N′-intermediate at 23.9 ppm, and the O-intermediate at 16.1 ppm all increased. We discuss the assignment of the N′- and O-intermediates in a later section. The ^{13}C CP-MAS NMR signals of the [20-^{13}C] retinal-*p*pR/*p*HtrII complex show the process of transforming from the G state (13.5 ppm) to a number of photointermediates. We previously reported that the G state was transformed to three kinds of M-intermediates (M1, M2, and M3) upon illumination with green light at −20°C (29). In this experiment, at −40°C, we observed photointermediates in the 13-*cis* form (22.9, 22.1, and 23.8 ppm), which were assigned to M1, M2, and N′-intermediate, respectively. The signal at 23.8 ppm was previously assigned to M3-intermediate. The photointermediate in the 13-*trans* form (16.1 ppm) was assigned to the O-intermediate. In summary, the 13-*trans* form product peak at 16.1 ppm can be assigned to the O-intermediate, and the 13-*cis* form can be assigned to the M-intermediates (22.1, 22.9 ppm) and the N′-intermediate (23.9 ppm), as discussed below. The chemical shift values are summarized in Table 1.

Relaxation process from the green-light irradiation state to the short dark state

The green-light-irradiation state was relaxed to the dark state by the process of thermal relaxation. Fig. 3 *Ac* and Fig. S1 *Ac* for full spectrum show the ^{13}C CP-MAS NMR spectrum of *p*pR/*p*HtrII complex obtained one day after terminating green-light irradiation. The difference spectrum shown in Fig. 3 *Be* and Fig. S1 *Ae* for full spectrum was obtained by

TABLE 1 ^{13}C Chemical Shift Values of Retinal Obtained from NMR Experiments

		Chemical Shift [ppm]		
		20-^{13}C	14-^{13}C	Configuration
*p*pR/*p*HtrII(−40°C)	G state	13.5 ± 0.8	–	13-*trans*, 15-anti
–	O-intermediate	16.1 ± 1.1	–	13-*trans*
–	M-intermediate	22.1, 22.9 ± 1.2	–	13-*cis,* 15-anti
–	N′-intermediate	23.9 ± 0.9	–	13-*cis*
*p*pR (−40°C)	G state	13.5 ± 0.7	121.7 ± 0.5	13-*trans*, 15-anti
–	M-intermediate	22.3 ± 1.3	126.8 ± 1.1	13-*cis,* 15-anti
*p*pR(−60°C)	G state	13.6 ± 1.5	121.6 ± 1.7	13-*trans,* 15-anti
–	O-intermediate	16.4 ± 1.3	115.4 ± 1.8	13-*trans*
–	M-intermediate	22.6 ± 1.2	127.1 ± 1.7	13-*cis,* 15-anti
–	N′-intermediate	23.9 ± 1.5	115.4 ± 1.2	13-*cis*

subtracting the initial dark state (*Dark1*) from the second short dark state (*Dark2*). The peak at 23.9 ppm remained unchanged, whereas the peaks at 22.1 and 22.9 ppm decreased in intensity. The difference spectrum shown in Fig. 3 *Bf* and Fig. S1 *Af* for full spectrum was obtained by subtracting the green-light-illumination state (*Green*) from the second short dark state (*Dark2*). The peaks at 22.1, 22.9, and 16.1 ppm decreased, and the G state increased in intensity. These results indicate that the peak at 23.9 ppm is not due to the M-intermediates but rather to the N′-intermediate, and therefore the half-lives of the M-intermediates at 22.1 and 22.9 ppm and of the O-intermediate at 16.1 ppm are much shorter than that of the N′-intermediate at 23.9 ppm. Therefore, we conclude that the M- and O-intermediates relaxed to the G state, and the N′-intermediate relaxed more slowly than the M- and O-intermediates.

Photoreaction pathway from the M-intermediates to the O-intermediate

An N-like intermediate with an absorbance maximum at 500 nm was previously observed in *p*pR in the 13-*cis* form in a transient absorption study (49) that used azide to accelerate the decay of the M-intermediates (50). To confirm the existence of this N-like intermediate, the sample in our study was irradiated with near-UV (blue) light at 365 nm to eliminate the M-intermediates (51), which have a maximal absorbance of 390 nm, after the accumulation of photointermediates by irradiation with 520 nm light.

Irradiation of the *p*pR/*p*HtrII complex with 520 nm green light at −40°C converted the G state to the O-, M-, and N′-intermediates (Fig. 3 *Bd* and Fig. 4 *Aa*). We found that the signal at 23.9 ppm did not decay upon irradiation with 365 nm light (Fig. 4 *Ab*). As described above, M-intermediates have an absorbance maximum at 390 nm due to the deprotonated SB. Therefore, M-intermediates immediately decay upon illumination with 365 nm blue light (51), and thus the remaining signal corresponding to the 13-*cis* form is assigned to the N′-intermediate (23.9 ppm).

After the M-intermediates of the *p*pR/*p*HtrII complex were trapped at −40°C in a stationary manner by illumination with green light (Fig. 4 *Aa*), irradiation with LED light at 520 nm was switched to 365 nm (Fig. 4 *Ab*). During this process, the intensities of the M-intermediates decayed and the intensities of the O-intermediate and the G state increased (Fig. 4 *Ac*), whereas the N′-intermediate did not decay over the same period (Fig. 4 *Ab*). Furthermore, it is noted that the M-intermediates were transformed to the O-intermediate after irradiation with 365 nm blue light (Fig. 4 *Ac*). The M-intermediates are reportedly transformed back to the G state by irradiation with blue light (365 nm) (51), because the M-intermediates have a maximal

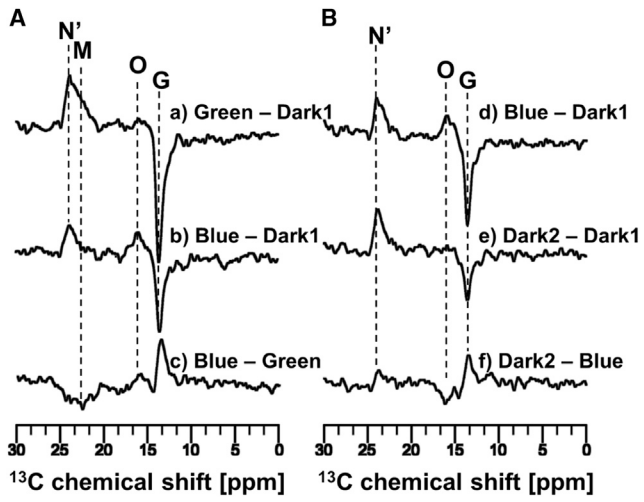

FIGURE 4 ^{13}C CP-MAS NMR difference spectra of the [20-^{13}C] retinal labeled *p*pR/*p*HtrII complex were measured at −40°C using 4 kHz MAS. (*Aa*) The difference spectrum obtained by subtracting the initial dark conditions (*Dark1*) from the green-light (520 nm)-illumination state (*Green*) (*Green* − *Dark1*) is shown. (*b*) The difference spectrum obtained by subtracting the initial dark conditions (*Dark1*) from the blue-light (365 nm)-illumination state (*Blue*) after the green-light stationary state (*Blue* − *Dark1*) is shown. (*c*) The difference spectrum obtained by Blue − Green, which is identical to (*b*) − (*a*), is shown. (*Bd*) The difference spectrum obtained by subtracting Dark1 from Blue (*Blue* − *Dark1*) is shown. (*e*) The difference spectrum obtained by subtracting Dark1 from the second dark condition (*Dark2*) after turning off irradiation (*Dark2* − *Dark1*) is shown. (*f*) The difference spectrum obtained by subtracting Blue from Dark2 (*Dark2* − *Blue*), which is identical to (*e*) − (*d*), is shown.

absorption of 390 nm. However, it was found in this experiment that the M-intermediates are transformed to the O-intermediate upon irradiation with 365 nm blue light (Fig. 4 *Ac*). As described above, spectroscopic evidence for the formation of an N′-intermediate was recently obtained in a transient absorption study (50), which reported that decay of the M-intermediates does not directly produce the N′-intermediate but rather produces an O-intermediate that is in equilibrium with the N′-intermediate. Based on previously reported findings and the results of this in situ photoirradiation solid-state NMR experiments, we summarize the photoreaction cycle of the *p*pR/*p*HtrII complex as follows (Fig. 5). The M-intermediates are converted to the O-intermediate under irradiation with 365 nm blue light through a double-photon process, and the O-intermediate is then converted to the N′-intermediate until an equilibrium state is achieved in which the intensity of the N′-intermediate is higher than that of the O-intermediate (Fig. 4 *Ab*).

It has been reported that the M-intermediate is converted to *p*pR′-intermediate at low temperatures of −160°C under near-UV-light irradiation and then back to *p*pR-state (52). This kind of *p*pR′-intermediate was not able to be accumulated at −40 and −60°C in this experiment. Moreover, the possibility that ^{13}C NMR signals of *p*pR′-intermediate are completely overlapped with those of *p*pR has not been ruled out, and thus *p*pR′-intermediate is not identified in this experiment.

Double-photon process from the G state to the O-intermediate

We identified the transformation process from the G state to the O-intermediate by observing the difference in the ^{13}C CP-MAS spectrum upon the blue-light (365 nm) irradiation of the G state. The ^{13}C CP-MAS NMR spectral measurement of the [20-^{13}C] retinal-*p*pR/*p*HtrII complex was first performed under initial dark conditions (*Dark1*) at −40°C. Upon switching directly from the initial dark condition (*Dark1*) to 365 nm blue-light illumination, the M-intermediates were converted to the O-intermediate through a double-photon process (Fig. 4 *Bd*). Consequently, the O-intermediate was converted to the N′-intermediate until an equilibrium state was reached (Fig. 4 *Be*). This pathway was clearly observed in the difference spectrum generated by subtracting the blue-light (365 nm)-illumination state from the Dark2 state (Fig. 4 *Bf*).

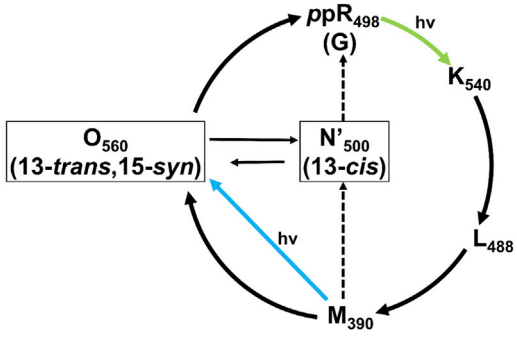

FIGURE 5 The photoreaction pathway of *p*pR including the N′-intermediate, as revealed by in situ photoirradiation solid-state NMR measurements. The O-intermediate is in an equilibrium state with the N′-intermediate. The λ maximum of the N′-intermediate was estimated at 500 nm (50). The transition process from the M-intermediates to the O-intermediate is shown by a straight arrow. The pathway for thermal relaxation from the M-intermediates to the N′-intermediate, and subsequently from the N′-intermediate to the G state, remains unclear and thus is designated with a black dashed arrow. The general configurations of the O- and N′-intermediates were the 13-*trans*, 15-*syn*, and the 13-*cis* forms, respectively. To see this figure in color, go online.

Photoreaction pathways of *p*pR from the G state to the M-intermediates at −40°C

We obtained the ^{13}C CP-MAS NMR signals of [20-^{13}C] retinal-*p*pR without *p*HtrII reconstituted in egg-PC under the initial dark conditions (Fig. 6 *Aa*) followed by green-light illumination with a 520 nm LED (Fig. 6 *Ab*). The difference spectrum (Fig. 6 *Ac*) between the M-intermediates and the G state (Fig. 6 *Aa* and *b*) indicated the transformation process from the G state to the M-intermediate.

The ^{13}C CP-MAS NMR spectra of [20-^{13}C] retinal-*p*pR under the green-light illumination with a 520 nm LED (Fig. 6 *Bd*) and in the subsequent dark condition (*Dark2*) (Fig. 6 *Be*) and the difference spectrum (Fig. 6 *Bf*) between the Dark2 condition and the green-light condition (Fig. 6 *Bd* and *e*) indicated that the M-intermediate transformed to the G state via a thermal-relaxation decay process at −40°C in *p*pR alone.

The ^{13}C NMR spectra of [14-^{13}C] retinal-*p*pR (Fig. 6, *C* and *D*) and the difference spectrum also indicated the process G state → M-intermediate → G state, as for [20-^{13}C] retinal-*p*pR. In addition, the chemical shift values of [14-^{13}C] retinal-*p*pR were 121.7 ppm (G state) and 126.8 ppm (M-intermediate) at −40°C (Table 1).

Photoreaction pathways from the M-intermediate to the O-intermediate in *p*pR

The M-, N′-, and O-intermediates were observed under continuous green-light (520 nm) illumination at −40°C using *p*pR/*p*HtrII complex. In contrast to the case of *p*pR/*p*HtrII, in the *p*pR alone, the N′- and O-intermediates could not be trapped at −40°C, indicating shorter half-lives than those of the *p*pR/*p*HtrII complex. As expected, these intermediates were successfully trapped at −60°C (Fig. 7 *Aa*).

In situ photoirradiation solid-state ^{13}C CP-MAS measurements were performed on [20-^{13}C] retinal-*p*pR alone at −60°C. Under illumination with green light, the difference ^{13}C CP-MAS NMR spectrum of [20-^{13}C] retinal-*p*pR (green-light illumination (*Green*) − initial dark condition (*Dark1*)) indicated the transformation process from the G

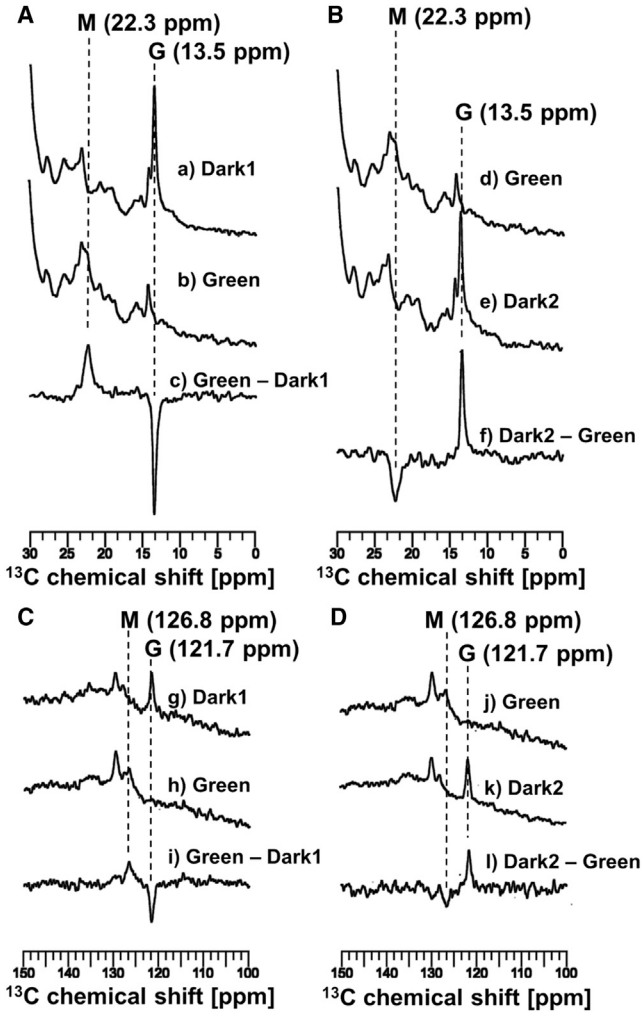

FIGURE 6 ^{13}C CP-MAS NMR spectra of [20-^{13}C, 14-^{13}C] retinal-*pp*R without *p*HtrII at −40°C under 4 kHz MAS. (*A*) The ^{13}C NMR spectra of [20-^{13}C] retinal-*pp*R indicating the transformation process from the G state (13.5 ppm) to the M-intermediate (22.3 ppm), (*a*) acquired under initial dark conditions (*Dark1*) and (*b*) acquired under green-light (520 nm)-illumination states (*Green*), and (*c*) the difference spectrum obtained by subtracting Dark1 from Green (*Green* − *Dark1*) are shown. (*B*) The ^{13}C NMR spectra of [20-^{13}C] retinal-*pp*R showing the thermal relaxation process from the M-intermediate to the G state, (*d*) acquired under green-light-illumination states (*Green*) and (*e*) acquired under short dark conditions (*Dark2*) after turning off irradiation, and (*f*) the difference spectrum obtained by subtracting Green from Dark2 (*Dark2* − *Green*) are shown. (*C*) The ^{13}C NMR spectra showing the region from 100.0 to 150.0 ppm for the same experiment as (*A*), (*g*) acquired under initial dark conditions (*Dark1*) and (*h*) acquired under green-light-illumination states (*Green*), and (*i*) the difference spectrum obtained by subtracting Dark1 from Green (*Green* − *Dark1*) are shown. (*D*) The ^{3}C NMR spectra showing the region from 100.0 to 150.0 ppm for the same experiment as (*B*), (*j*) acquired under green-light-illumination states (*Green*) and (*k*) acquired under short dark conditions (*Dark2*) after turning off irradiation, and (*l*) the difference spectrum obtained by subtracting Green from Dark2 (*Dark2* − *Green*) are shown. The spectra shown in (*C* and *D*) indicate the transformation process from the G state (121.7 ppm) to the M-intermediate (126.8 ppm) and the thermal decay process.

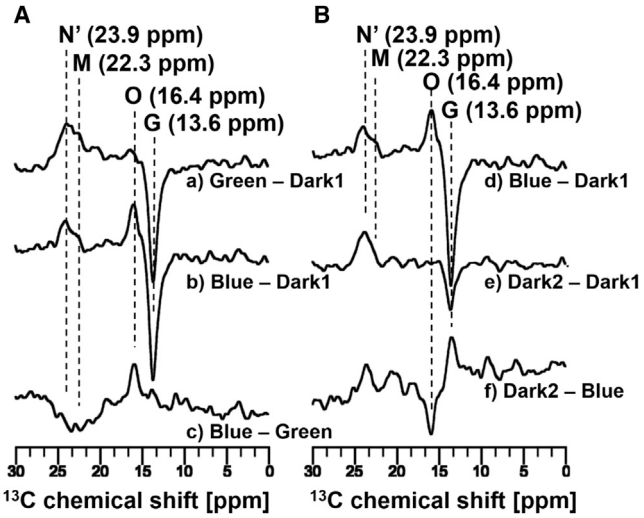

FIGURE 7 ^{13}C CP-MAS NMR signals of [20-^{13}C] retinal-*pp*R alone at −60°C under 4 kHz MAS. (*A*) The difference spectra of the [20-^{13}C] retinal-*pp*R were obtained (*a*) by subtracting the initial dark conditions (*Dark1*) from the green-light-illumination (520 nm) state (*Green*) (*Green* − *Dark1*); (*b*) by subtracting Dark1 from the blue-light (365 nm)-illumination state (*Blue*) (*Blue* − *Dark1*); and (*c*) by subtracting Green from Blue (*Blue* − *Green*). The difference spectrum shown in (*a*) indicates the transformation process from the G state (13.6 ppm) to the M- (22.3 ppm), N′- (23.9 ppm), and O-intermediates (16.4 ppm) upon green-light (520 nm) illumination. The difference spectra shown in (*b*) and (*c*) indicate that the O-intermediate (16.4 ppm) was trapped upon the subsequent blue-light (365 nm) illumination. (*B*) The difference spectra of [20-^{13}C] retinal-*pp*R obtained (*d*) by subtracting Dark1 from Blue (*Blue* − *Dark1*); (*e*) by subtracting Dark1 from the short dark conditions after turning off irradiation (*Dark2*) (*Dark2* − *Dark1*); and (*f*) by subtracting Blue from Dark2 (*Dark2* − *Blue*) are shown.

state (13.6 ppm) to the O-, M-, and N′-intermediates (16.4, 22.3, and 23.9 ppm) (Fig. 7 *Aa*). After stationary trapping of these photointermediates, the light source was switched from 520 to 360 nm. The result indicated that the signal of the M-intermediates (22.6 ppm) decreased and the signal of the O-intermediate (16.4 ppm) increased (Fig. 7 *Ab*). The absorbance maximum of the M-intermediate was 395 nm, and thus this result indicated that the M-intermediates were transformed to the O-intermediate by irradiation with 365 nm blue light (Fig. 7 *Ac*).

Relaxation process from the O-intermediate to the N′-intermediate

We obtained the relaxation process from the O-intermediate to the N′-intermediate from the difference spectra shown in Fig. 7 *B*. The difference ^{13}C CP-MAS NMR spectrum of [20-^{13}C] retinal-*pp*R between the blue (365 nm) state (*Blue*) and initial dark conditions (*Dark1*) indicated that the product photointermediates were the O- and N′-intermediates in the blue-light (365 nm)-illumination state. By turning off the irradiation, the O-intermediate was converted to the N′-intermediate, as with the *pp*R/*p*HtrII complex

(Fig. 7 *Be*). This pathway was clearly observed in the difference spectrum generated by subtracting the blue-light (365 nm)-illumination state from the Dark2 state (Fig. 7 *Bf*).

Chemical shift values of [14-^{13}C] retinal for the intermediates in *p*pR

We revealed the configurations of the O- and N′-intermediate by measuring the ^{13}C CP-MAS NMR spectra of [14-^{13}C] retinal-*p*pR. The chemical shift values of [14-^{13}C] retinal contain important information regarding the 15-*syn*/anti configuration (20,33). The spectra shown in Fig. 8 show the region from 100.0 to 150.0 ppm for the same experiments as shown in Fig. 7 and indicate the chemical shifts of [14-^{13}C] retinal-*p*pR. At −60°C, in situ photoirradiation solid-state ^{13}C CP-MAS spectra were observed for [14-^{13}C] retinal-*p*pR, and the signal at 127.1 ppm was assigned to [14-^{13}C] retinal in the M-intermediates resulting from a transformation process from the G state to the M-intermediates under green-light (520 nm) illumination (Fig. 8 *Aa*). Subsequent blue-light (365 nm) illumination resulted in an intense signal from the O-intermediate, as with the signal of [20-^{13}C] retinal-*p*pR shown in Fig. 7. Therefore, the main positive peak in the difference spectrum (Fig. 8 *Ab*) was assigned to the O-intermediate, and the chemical shift value of [14-^{13}C] retinal was 115.4 ppm. As discussed above, the M-intermediates transform to the O-intermediate upon blue-light (365 nm) illumination, and thus the chemical shift value at 115.4 ppm was indeed due to the O-intermediate (Fig. 8 *Ac*). The spectrum shown in Fig. 8 *Bd* also indicated that the 115.4 ppm signal is assignable to the O-intermediate because of the double photon process from the G state to the O-intermediate upon blue-light (365 nm) illumination.

The difference spectrum shown in Fig. 8 *Be* clearly indicated that the 115.4 ppm signal also belonged to the N′-intermediate, because the N′-intermediate showed a very long half-life and the signal intensity remained unchanged at −60°C, as shown in Fig. 7*b* and *e*. In addition, the thermal relaxation pathway of the O-intermediate was observed as a decrease in the signal at 115.4 ppm (Fig. 8 *Bf*).

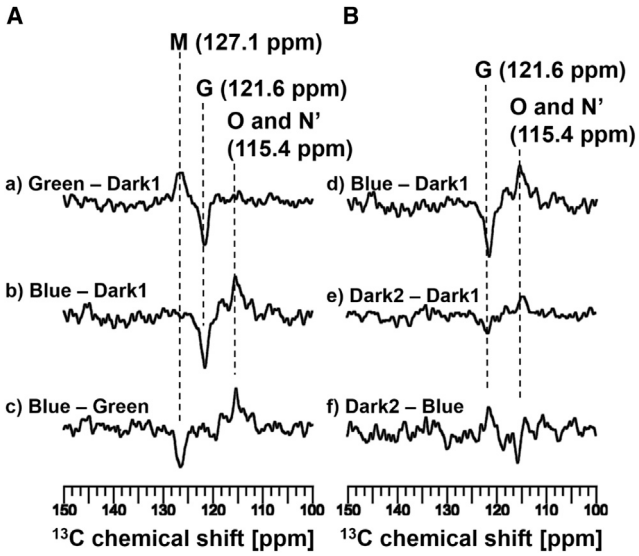

FIGURE 8 ^{13}C CP-MAS NMR signals of [14-^{13}C] retinal-*p*pR alone at −60°C under 4 kHz MAS. (*A*) The difference spectra of [14-^{13}C] retinal-*p*pR obtained (*a*) by subtracting the initial dark conditions (*Dark1*) from the green-light (520 nm)-illumination states (*Green*) (*Green − Dark1*); (*b*) by subtracting Dark1 from the blue-light (365 nm)-illumination state (*Blue*) (*Blue − Dark1*); and (*c*) subtracting Green from Blue (*Blue − Green*) are shown. The difference spectrum shown in (*a*) indicates the transformation process from the G state (121.6 ppm) to the M-intermediates (127.1 ppm) upon green-light (520 nm) illumination. The difference spectra shown in (*b*) and (*c*) indicate the transition process from the M-intermediates to the O-intermediate (115.4 ppm) upon subsequent blue-light (365 nm) illumination. (*B*) The difference spectra of [14-^{13}C] retinal-*p*pR obtained (*d*) by subtracting Dark1 from Blue (*Blue − Dark1*); (*e*) by subtracting Dark1 from the short dark conditions after turning off irradiation (*Dark2*) (*Dark2 − Dark1*); and (*f*) by subtracting Blue from Dark2 (*Dark2 − Blue*) are shown. The difference spectra shown in (*e*) and (*f*) indicate that the remaining signal at 115.4 ppm belongs to the N′-intermediate.

Conformation of retinal in the late photointermediates

We have assigned the ^{13}C NMR chemical shift values for the late photointermediates M-, O-, and N′-intermediates (Table 1). The configuration of the M-intermediates was clearly shown to be 13-*cis*, 15-anti by comparing this result with previous studies of *Salinibacter* sensory rhodopsin I (SrSRI), bR, and its mutant Y185F-bR (20,30,33) (Table S1). Furthermore, the deprotonated SB state in the M-intermediates was obtained as a result of the fast transformation process initiated by blue-light (365 nm) illumination. This comparison and our previous studies in *p*pR and SrSRI (30,31) allow the 13C=14C configuration of retinal in the O- and N′-intermediates to be assigned to the 13-*trans* and 13-*cis* forms, respectively. The 15C=Nζ configuration is more challenging, because the value of 115.4 ppm is the boundary region between the 15-*syn* and 15-anti forms. For example, in the study of Y185F-bR, the CS* intermediate has been assigned to the 15-*syn* form, and the chemical shift value of [14-^{13}C] retinal was 115.3 ppm (33). On the other hand, the N-intermediate of wild-type bR has been assigned to the 15-anti form, and the chemical shift value of [14-^{13}C] retinal was 115.2 ppm (53) (Table S1). The following is a detailed discussion of the configurations of the O- and N′-intermediates as elucidated by DFT calculation.

Determination of the dihedral angles *Φ* for the O- and N′-intermediates

We elucidated the configuration of the O- and N′-intermediates by investigating the relationship between the ^{13}C NMR chemical shift values and configuration by using DFT calculation. The crystal structure (PDB: 1JGJ) (48)

corresponding to the G state was used as a starting configuration and has the dihedral angles $\Phi = -177$, $\Psi = -175$, and X $= -66°$. The chemical shift values of 20-^{13}C and 14-^{13}C for this configuration were calculated to be 17.5 and 128.1 ppm, respectively, and these values are shown in Table 2. Touw et al. (54) previously calculated the chemical shift at 20-^{13}C for all-*trans* retinal to be 18.0 ppm (54), which is very similar to the value obtained in this work. However, these calculated values show some discrepancy with the experimental values of 13.6 and 121.6 ppm, with the calculated chemical shift values being 3.9 and 6.5 ppm larger than the experimental 20-^{13}C and 14-^{13}C values, respectively. Touw et al. (54) also showed a similar discrepancy. Therefore, in the following discussion, the calculated values will be discussed with corrected values by adding 3.9 and 6.5 ppm to the experimental values for 20-^{13}C and 14-^{13}C in retinal, respectively.

The dependence of the chemical shift value of 20-^{13}C in retinal on the dihedral angles Φ and Ψ were investigated, and the results are shown in Fig. 9, *A* and *B*, respectively. The chemical shift at 20-^{13}C in retinal drastically changes according to the rotation of dihedral angle Φ, but it is almost independent of the change in the dihedral angle Ψ. These results indicate that the value of 20-^{13}C can be used to determine the configuration with dihedral angle Φ. The experimental chemical shift values of 20-^{13}C for the O- and N′-intermediates were 16.4 and 23.9 ppm, and thus the corrected values of these conformations should be 20.3 and 27.8 ppm, respectively. The positions of these values are shown in Fig. 9 *A*. The corresponding dihedral angle Φ for the O-intermediate configuration was estimated as $-150°$, and for the N′-intermediate it was estimated as $-63°$, as shown in Table 2.

Determination of the dihedral angle Ψ for the O-intermediate

The dihedral angle Φ in the O-intermediate was estimated to be $-150°$, and thus the dihedral angle Ψ was investigated for this intermediate next. The dependence of the chemical shift value of 14-^{13}C in retinal on the dihedral angle Ψ was evaluated by setting Φ at $-150°$ and X at $-66°$. The results

TABLE 2 ^{13}C Chemical Shift Values of Retinal Calculated by DFT and the Conformation of Retinal in Several Photointermediates

	Chemical Shift [ppm]		Dihedral Angle [degree]			
	20-^{13}C	14-^{13}C	Φ	Ψ	X	Configuration
G state	17.5	128.1	−177[a]	−175[a]	−66[a]	13-*trans*, 15-anti
O-intermediate	20.3	121.9	−150	0	−180	13-*trans*, 15-*syn*
N′-intermediate	27.8	121.9	−63	−175	−180	13-*cis*, 15-anti
				−7	−180	13-*cis*, 15-*syn*
				−175	−66[a]	13-*cis*, 15-anti

[a](48) (PDB: 1JGJ).

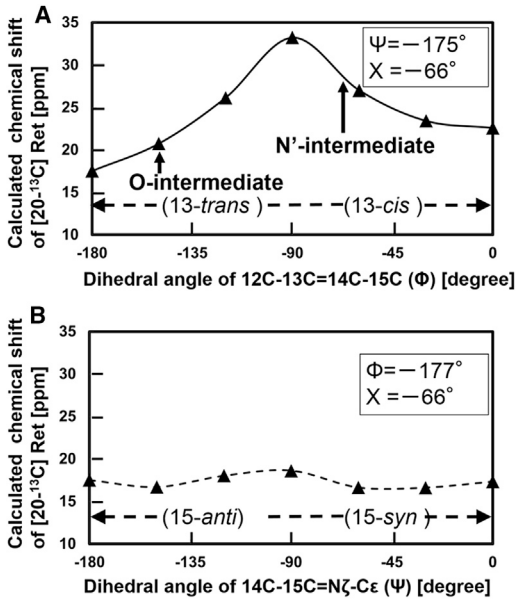

FIGURE 9 The dependency of the chemical shift value of 20-^{13}C in retinal on the dihedral angles Φ and Ψ is shown in (*A*) and (*B*), respectively. In (*A*), only the dihedral angle Φ was rotated from the *trans* ($-180°$) to the *cis* (0°) configuration by setting Ψ and X at -175 and $-66°$, respectively (48). In (*B*), only the dihedral angle Ψ was rotated from the anti ($-180°$) to the *syn* (0°) configuration by fixing Φ and X to -177 and $-66°$, respectively (48). The calculated chemical shift values were converted to ppm from TMS.

are shown in Fig. 10 (*dashed line*) and indicate that the chemical shift value for the 15-*syn* form was larger than that of the 15-anti form. However, previous experiments showed the opposite. For example, the values of 14-^{13}C for 15-anti and 15-*syn* were 122.0 and 110.5 ppm for bR as shown in Table S1, and thus the calculated chemical shift of the *syn*-state should be upfield compared to that of the anti-state.

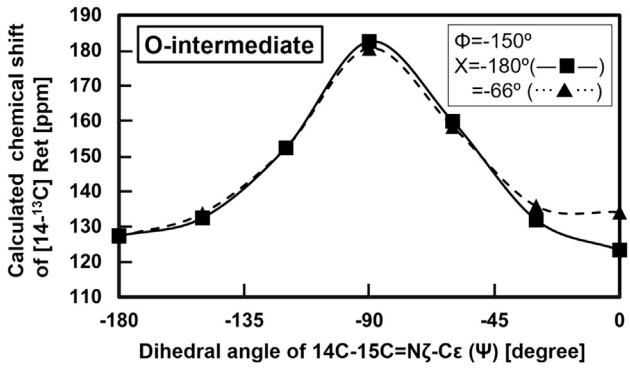

FIGURE 10 The chemical shift value of 14-^{13}C in retinal was calculated by changing the dihedral angle Ψ. The Φ angle was fixed at $-150°$, as estimated for the O-intermediate conformation discussed in Fig. 9. The X angle was set at the crystal conformation (48) of $-66°$ in (▲), and the *trans* conformation (48) of $-180°$ in (X).

We resolved this discrepancy by conducting calculations using the *trans* configuration for dihedral angle X (X = −180°), because in this configuration, we would expect a γ-effect between the 14-^{13}C proton and the ε proton (55). The results are also shown in Fig. 10 and indicate that the chemical shift value of 14-^{13}C in the *syn* conformation (Ψ = 0°) changed by −4.0 ppm from anti (Ψ = −180°) configuration (Fig. 10, *dashed line*). This change in chemical shift allowed estimation of the configuration of the O-intermediate. The experimental chemical shift value of 14-^{13}C of the O-intermediate was 115.4 ppm, as summarized in Table 1, and thus the offset value of this configurations should be 121.9 ppm, corresponding to a dihedral angle Ψ of 0°. The configuration of the O-intermediate can thus be determined to have the dihedral angles Φ and Ψ of −150 and 0°, respectively, as listed in Table 2. These results indicated that the configuration of the O-intermediate was, in general, in the 13-*trans* and 15-*syn* form.

Determination of the dihedral angle Ψ for the N′-intermediate

The dihedral angle of Ψ was estimated in a manner similar to that discussed above. The conformation of the N′-intermediate was calculated using the dependence of the chemical shift value of 14-^{13}C in retinal on the dihedral angle Ψ, and the results are shown in Fig. 11. The dihedral angle Φ in the N′-intermediate was set at −63° as estimated in Fig. 9 *A*. Two sets of values were used in the calculations for the dihedral angle X: the crystal value of −66° and the *trans* form value of −180°, and both the results are shown in Fig. 11. The curves of the chemical shifts allowed estimation of the conformation of the N′-intermediate. The chemical shift value of 14-^{13}C of the N′- intermediate was 115.4 ppm, as summarized in Table 1, and thus the offset value of this conformation should be 121.9 ppm. However, three points correspond to the dihedral angle Ψ in Fig. 11: the dihedral angles Ψ and X are (Ψ = −175° and X = −66°), (Ψ = −175° and X = −180°), and (Ψ = −17° and X = −180°). Although the dihedral angle Φ in the N′-intermediate was determined as −63°, the remaining dihedral angles Ψ and X could be any of these three possibilities.

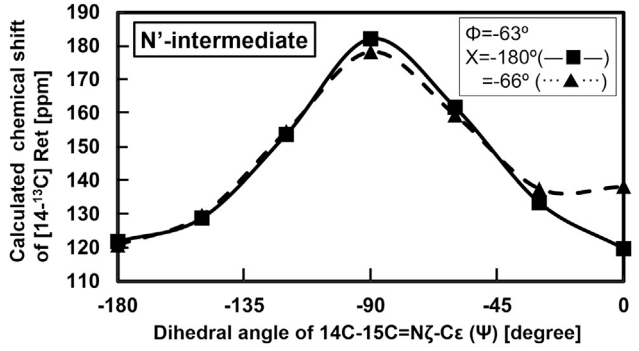

FIGURE 11 The chemical shift value of 14-^{13}C in retinal was calculated by changing the dihedral angle Ψ and fixing Φ at −63°, as estimated for the N′-intermediate configuration discussed in Fig. 9. The X angle was set at the crystal configuration (48) of −66° in (▲), and the *trans* conformation (48) of −180° in (X).

CONCLUSIONS

It is demonstrated that in situ photoirradiation solid-state NMR spectroscopy allows us to observe the photointermediates in the stationary state and determine the photoreaction pathways of photoreceptor membrane proteins such as the *p*pR/*p*HtrII complex system to gain insight into the signal transduction mechanism.

We observed the M-, O-, and N′-intermediates from *p*pR and *p*pR/*p*HtrII complex reconstituted in egg-PC membrane by irradiation with green light using in situ photoirradiation solid-state NMR. Changes in the ^{13}C CP-MAS NMR signals resulting from switching the wavelength of light used for continuous irradiation from green light (520 nm) to blue light (365 nm) revealed the pathways of the late photoactive intermediates from the M-intermediates to the O-intermediate. Interestingly, one of the multiple M-intermediates previously reported was identified as an N-like intermediate reported in bR, which we designated the N′-intermediate. The N′-intermediate is produced from the O-intermediate in *p*pR, whereas the N-intermediate is produced from M-intermediate in bR. This result indicates that large structural changes of the proteins are necessary to produce the N′-intermediate, which is in an equilibrium state with the O-intermediate. In addition, the half-life of the N′-intermediate for the ppR/pHtrII complex was shown to be longer than that for *p*pR. In the physiological point of view, we suggested that the N′-intermediate might play important role in signaling processes as a preamplitude mechanism because it has a long half-life and is in equilibrium with the O-intermediate. Detailed configurations of the O- and N′-intermediates were revealed to be 13-*trans*, 15-*syn*, and 13-*cis*, respectively, by NMR experiments and DFT calculation and showed that the chemical shift values of [14-^{13}C] retinal are useful for determining the 15-*syn* or 15-anti configuration. The results of our DFT calculation are the first step of the trial to find the conformation of the intermediate states of the retinal, which would be difficult to get only from the experimental work. Further refinement of the calculation will be needed to confirm the proposed intermediate conformations in future.

SUPPORTING MATERIAL

One figure and two tables are available at http://www.biophysj.org/biophysj/supplemental/S0006-3495(18)30669-6.

AUTHOR CONTRIBUTIONS

Y.M. performed NMR measurements, DFT calculation, and analyses, and wrote the article. I.K. and A.N. designed NMR experiments and wrote

the article. K.U. performed DFT calculation and wrote the article. T.O. and A.W. prepared labeled retinal. N.K. and Y.S. designed sample preparation and gave valuable discussion on the article.

ACKNOWLEDGMENTS

This work was supported by Grants-in-Aid for Scientific Research in an Innovative Area (16H00756 to A.N., 25104005 to Y.S., and 16H00828 to I.K.), a Grant-in-Aid for Scientific Research (C) (15K06963 to A.N.) and Research (B) (15H04363 to Y.S. and 15H04336 to I.K.), and a Grant-in-Aid for Japan Society for the Promotion of Research as Research Fellowship (16J00073 to Y.M.) from the Ministry of Culture, Sports, Science and Technology of Japan. This work was also supported by the Japan Society and Technology-CREST and the Japan Agency for Medical Research and Development grants to Y.S. The authors thank the Research Center for Computational Science, Okazaki, Japan, for use of their computing facilities to perform a part of the calculation described in this work.

REFERENCES

1. Govorunova, E. G., O. A. Sineshchekov, …, J. L. Spudich. 2017. Microbial Rhodopsins: diversity, mechanisms, and optogenetic applications. *Annu. Rev. Biochem.* 86:845–872.
2. Hoff, W. D., K. H. Jung, and J. L. Spudich. 1997. Molecular mechanism of photosignaling by archaeal sensory rhodopsins. *Annu. Rev. Biophys. Biomol. Struct.* 26:223–258.
3. Spudich, J. L., and H. Luecke. 2002. Sensory rhodopsin II: functional insights from structure. *Curr. Opin. Struct. Biol.* 12:540–546.
4. Suzuki, D., H. Irieda, …, Y. Sudo. 2010. Phototactic and chemotactic signal transduction by transmembrane receptors and transducers in microorganisms. *Sensors (Basel).* 10:4010–4039.
5. Inoue, K., T. Tsukamoto, and Y. Sudo. 2014. Molecular and evolutionary aspects of microbial sensory rhodopsins. *Biochim. Biophys. Acta.* 1837:562–577.
6. Kamo, N., K. Shimono, …, Y. Sudo. 2001. Photochemistry and photo-induced proton-transfer by pharaonis phoborhodopsin. *Biochemistry (Mosc.).* 66:1277–1282.
7. Imamoto, Y., Y. Shichida, …, T. Yoshizawa. 1992. Chromophore configuration of pharaonis phoborhodopsin and its isomerization on photon absorption. *Biochemistry.* 31:2523–2528.
8. Gordeliy, V. I., J. Labahn, …, M. Engelhard. 2002. Molecular basis of transmembrane signalling by sensory rhodopsin II-transducer complex. *Nature.* 419:484–487.
9. Moukhametzianov, R., J. P. Klare, …, V. I. Gordeliy. 2006. Development of the signal in sensory rhodopsin and its transfer to the cognate transducer. *Nature.* 440:115–119.
10. Ishchenko, A., E. Round, …, V. Gordeliy. 2017. New insights on signal propagation by sensory rhodopsin II/transducer complex. *Sci. Rep.* 7:41811.
11. Shimono, K., T. Hayashi, …, N. Kamo. 2003. Importance of the broad regional interaction for spectral tuning in Natronobacterium pharaonis phoborhodopsin (sensory rhodopsin II). *J. Biol. Chem.* 278:23882–23889.
12. Sudo, Y., Y. Furutani, …, J. L. Spudich. 2006. Functional importance of the interhelical hydrogen bond between Thr^{204} and Tyr^{174} of sensory rhodopsin II and its alteration during the signaling process. *J. Biol. Chem.* 281:34239–34245.
13. Sudo, Y., Y. Furutani, …, H. Kandori. 2005. Steric constraint in the primary photoproduct of an archaeal rhodopsin from regiospecific perturbation of C-D stretching vibration of the retinyl chromophore. *J. Am. Chem. Soc.* 127:16036–16037.
14. Wegener, A. A., I. Chizhov, …, H. J. Steinhoff. 2000. Time-resolved detection of transient movement of helix F in spin-labelled pharaonis sensory rhodopsin II. *J. Mol. Biol.* 301:881–891.
15. Spudich, J. L. 1998. Variations on a molecular switch: transport and sensory signalling by archaeal rhodopsins. *Mol. Microbiol.* 28:1051–1058.
16. Yoshida, H., Y. Sudo, …, N. Kamo. 2004. Transient movement of helix F revealed by photo-induced inactivation by reaction of a bulky SH-reagent to cysteine-introduced pharaonis phoborhodopsin (sensory rhodopsin II). *Photochem. Photobiol. Sci.* 3:537–542.
17. Ernst, O. P., D. T. Lodowski, …, H. Kandori. 2014. Microbial and animal rhodopsins: structures, functions, and molecular mechanisms. *Chem. Rev.* 114:126–163.
18. Smith, S. O., H. J. de Groot, …, R. G. Griffin. 1989. Structure and protein environment of the retinal chromophore in light- and dark-adapted bacteriorhodopsin studied by solid-state NMR. *Biochemistry.* 28:8897–8904.
19. McDermott, A. E., L. K. Thompson, …, R. G. Griffin. 1991. Mechanism of proton pumping in bacteriorhodopsin by solid-state NMR: the protonation state of tyrosine in the light-adapted and M states. *Biochemistry.* 30:8366–8371.
20. Farrar, M. R., K. V. Lakshmi, …, J. Herzfeld. 1993. Solid state NMR study of [ε-^{13}C]Lys-bacteriorhodopsin: Schiff base photoisomerization. *Biophys. J.* 65:310–315.
21. de Groot, H. J., S. O. Smith, …, J. Herzfeld. 1990. Solid-state ^{13}C and ^{15}N NMR study of the low pH forms of bacteriorhodopsin. *Biochemistry.* 29:6873–6883.
22. Hu, J. G., B. Q. Sun, …, J. Herzfeld. 1998. Early and late M intermediates in the bacteriorhodopsin photocycle: a solid-state NMR study. *Biochemistry.* 37:8088–8096.
23. Petkova, A. T., M. Hatanaka, …, J. Herzfeld. 2002. Tryptophan interactions in bacteriorhodopsin: a heteronuclear solid-state NMR study. *Biochemistry.* 41:2429–2437.
24. Hu, J. G., B. Q. Sun, …, J. Herzfeld. 1997. The predischarge chromophore in bacteriorhodopsin: a ^{15}N solid-state NMR study of the L photointermediate. *Biochemistry.* 36:9316–9322.
25. Mak-Jurkauskas, M. L., V. S. Bajaj, …, J. Herzfeld. 2008. Energy transformations early in the bacteriorhodopsin photocycle revealed by DNP-enhanced solid-state NMR. *Proc. Natl. Acad. Sci. USA.* 105:883–888.
26. Bajaj, V. S., M. L. Mak-Jurkauskas, …, R. G. Griffin. 2009. Functional and shunt states of bacteriorhodopsin resolved by 250 GHz dynamic nuclear polarization-enhanced solid-state NMR. *Proc. Natl. Acad. Sci. USA.* 106:9244–9249.
27. Becker-Baldus, J., C. Bamann, …, C. Glaubitz. 2015. Enlightening the photoactive site of channelrhodopsin-2 by DNP-enhanced solid-state NMR spectroscopy. *Proc. Natl. Acad. Sci. USA.* 112:9896–9901.
28. Kawamura, I., N. Kihara, …, A. Naito. 2007. Solid-state NMR studies of two backbone conformations at Tyr185 as a function of retinal configurations in the dark, light, and pressure adapted bacteriorhodopsins. *J. Am. Chem. Soc.* 129:1016–1017.
29. Tomonaga, Y., T. Hidaka, …, A. Naito. 2011. An active photoreceptor intermediate revealed by in situ photoirradiated solid-state NMR spectroscopy. *Biophys. J.* 101:L50–L52.
30. Yomoda, H., Y. Makino, …, A. Naito. 2014. Color-discriminating retinal configurations of sensory rhodopsin I by photo-irradiation solid-state NMR spectroscopy. *Angew. Chem. Int.Engl.* 53:6960–6964.
31. Naito, A., and I. Kawamura. 2014. Photoactivated structural changes in photoreceptor membrane proteins as revealed by in situ photoirradiation solid-state NMR spectroscopy. *In* Advances in Biological Solid-State NMR: Proteins and Membrane-Active Peptides. F. Separovic and A. Naito, eds. Royal Society of Chemistry, pp. 387–404.
32. Naito, A., I. Kawamura, and N. Javkhlantugs. 2015. Recent solid-state NMR studies of membrane-bound peptides and proteins. *Annu. Rep. NMR Spectrosc.* 86:334–411.
33. Oshima, K., A. Shigeta, …, A. Naito. 2015. Characterization of photointermediates in the photo-reaction pathways of a bacteriorhodopsin Y185F mutant using in situ photo-irradiation solid-state NMR spectroscopy. *Photochem. Photobiol. Sci.* 14:1694–1702.

34. Naito, A., Y. Makino, …, I. Kawamura. 2018. Photoirradiatiion and microwave irradiation NMR spectroscopy. *In* Experimental Approaches of NMR Spectroscopy. The Nuclear Magnetic Resonance Socirty of Japan, ed. Springer, pp. 135–170.
35. Naito, A., Y. Makino, and I. Kawamura. 2017. In-situ photo irradiation solid-state NMR spectroscopy applied to retinal-binding membrane proteins. *In* Modern Magnetic Resonance. G. A. Webb, ed. Springer, pp. 1–22.
36. Kitajima-Ihara, T., Y. Furutani, …, Y. Sudo. 2008. Salinibacter sensory rhodopsin: sensory rhodopsin I-like protein from a eubacterium. *J. Biol. Chem.* 283:23533–23541.
37. Kawamura, I., H. Yoshida, …, A. Naito. 2008. Dynamics change of phoborhodopsin and transducer by activation: study using D75N mutant of the receptor by site-directed solid-state ^{13}C NMR. *Photochem. Photobiol.* 84:921–930.
38. Sudo, Y., M. Yamabi, …, N. Kamo. 2003. Interaction of Natronobacterium pharaonis phoborhodopsin (sensory rhodopsin II) with its cognate transducer probed by increase in the thermal stability. *Photochem. Photobiol.* 78:511–516.
39. Schaefer, J., and E. O. Stejskal. 1976. Carbon-13 nuclear magnetic resonance of polymers spinning at the magic angle. *J. Am. Chem. Soc.* 98:1031–1032.
40. Bennett, A. E., C. M. Rienstra, …, R. G. Griffin. 1995. Heteronuclear decoupling in rotating solids. *J. Chem. Phys.* 103:6951–6958.
41. Saitô, H., I. Ando, and A. Ramamoorthy. 2010. Chemical shift tensor - the heart of NMR: insights into biological aspects of proteins. *Prog. Nucl. Magn. Reson. Spectrosc.* 57:181–228.
42. London, F. 1937. Théorie quantique des courants interatomiques dans les combinaisons aromatiques. *J. Phys. Radium.* 8:397–409.
43. Ditchfield, R. 1972. Molecular orbital theory of magnetic shielding and magnetic susceptibility. *J. Chem. Phys.* 56:5688–5691.
44. Ditchfield, R. 1974. Self-consistent perturbation theory of diamagnetism I. A gauge-invariant LCAO method for N.M.R. Chemical shifts. *Mol. Phys.* 27:789–807.
45. Woliński, K., and A. J. Sadlej. 1980. Self-consistent perturbation theory open-shell states in perturbation-dependent non-orthogonal basis sets. *Mol. Phys.* 41:1419–1430.
46. Wolinski, K., J. F. Hinton, and P. Pulay. 1990. Efficient implementation of the gauge-independent atomic orbital method for NMR chemical shift calculations. *J. Am. Chem. Soc.* 112:8251–8260.
47. Frisch, M. J., G. W. Trucks, …, J. A. Pople. 2004. Gaussian 09, Revision A.02. Gaussian, Inc., Wallingford, CT.
48. Luecke, H., B. Schobert, …, J. L. Spudich. 2001. Crystal structure of sensory rhodopsin II at 2.4 angstroms: insights into color tuning and transducer interaction. *Science.* 293:1499–1503.
49. Chizhov, I., G. Schmies, …, M. Engelhard. 1998. The photophobic receptor from Natronobacterium pharaonis: temperature and pH dependencies of the photocycle of sensory rhodopsin II. *Biophys. J.* 75:999–1009.
50. Tateishi, Y., T. Abe, …, M. Unno. 2011. Spectroscopic evidence for the formation of an N intermediate during the photocycle of sensory rhodopsin II (phoborhodopsin) from Natronobacterium pharaonis. *Biochemistry.* 50:2135–2143.
51. Roy, S., T. Kikukawa, …, N. Kamo. 2006. All-optical switching in Pharaonis phoborhodopsin protein molecules. *IEEE Trans. Nanobioscience.* 5:178–187.
52. Balashov, S. P., M. Sumi, and N. Kamo. 2000. The M intermediate of Pharaonis phoborhodopsin is photoactive. *Biophys. J.* 78:3150–3159.
53. Lakshmi, K. V., M. R. Farrar, …, J. Herzfeld. 1994. Solid state ^{13}C and ^{15}N NMR investigations of the N intermediate of bacteriorhodopsin. *Biochemistry.* 33:8853–8857.
54. Touw, S. I. E., H. J. M. De Groot, and F. Buda. 2004. DFT calculations of the ^{1}H chemical shifts and ^{13}C chemical shift tensors of retinal isomers. *J. Mol. Struct. THEOCHEM.* 711:141–147.
55. Harbison, G. S., S. O. Smith, …, R. G. Griffin. 1984. Dark-adapted bacteriorhodopsin contains 13-cis, 15-syn and all-trans, 15-anti retinal Schiff bases. *Proc. Natl. Acad. Sci. USA.* 81:1706–1709.